DOI: 10.1002/cjoc.201700220

Binuclear Ruthenium Complexes with Benzo[1,2-b;4,5-b']-dithiophene Analogues as Bridge Ligands: Syntheses, Characterization and Notable Difference on Electronic Coupling

Ya-Ping Ou,* Shunlin Tang, Aihui Wang, Junhua Li, Fuxing Zhang, and Zhifeng Xu

College of Chemistry and Material Science, *Hengyang Normal University*; *Key Laboratory of Functional Organometallic Materials of Hengyang Normal University*, *College of Hunan Province*, *Hengyang*, *Hunan 421008*, *China*

Diruthenium ethynyl complexes **1**—**3** (**1**: 1,5-dithia-s-indacene-4,8-dione; **2**: 4,8-diethoxybenzo[1,2-b:4,5-b']dithiophene; **3**: 4,8-didodecyloxybenzo[1,2-b:4,5-b']dithiophene) have been synthesized by incorporating the respective conjugated heterocyclic spacer and characterized by NMR and elemental analysis. The effects of bridge ligands' properties on electronic coupling between redox-active ruthenium terminal groups were investigated by electrochemistry, UV/vis/near-IR and IR spectroelectrochemistry combined with density functional theory (DFT) and time-dependent DFT calculations. Electrochemistry results indicated that complexes **1**—**3** exhibit two fully reversible oxidation waves, and complexes **2** and **3** with electron-rich and π-conjuagted bridge ligands are characterized by excellent electrochemical properties. Furthermore, the larger ν(C≡C) separation from the IR spectroelectrochemical results of **2** and **3** and the intense NIR absorption features of singly oxidized species $\mathbf{2}^+$ and $\mathbf{3}^+$ revealed that their molecular skeletons have superior abilities to delocalize the positive charge. The spin density distribution from DFT calculations proved the conclusions of this study.

Keywords bridge ligands, ruthenium terminal groups, spectroelectrochemistry, electronic coupling

Introduction

Binuclear complexes that contain two redox-active metal terminals and π-conjugated bridge ligands as models have been proven to be useful for the design and research of molecular wires, the methods have been extensively applied in recent years to explore the electronic transport ability of bridge ligands based on the electronic communications between two redox-active metal terminals.[1-4] Recently, numerous organic conjugative ligands and redox-active metal terminals were used to develop a type of "organometallic molecular wires" model.[4] Organic bridge ligands in these complexes are usually rich in electrons, which can provide an electronic coupling pathway; some representative examples are polyene,[5] polyyne,[6] oligomeric aromatic hydrocarbons,[7] polycyclic aromatic hydrocarbons,[8] and heteroacenes.[9] As for the metal terminal groups, iron,[10] ruthenium,[7,8,11] osmium,[12] and molybdenum[13] units with different auxiliary ligands, such as cyclopentadienyl, bis(diphenylphosphino)ethane (dppe) are typically used because of their redox-active properties and electrochemical stability.

Dimetallic systems with the above mentioned ruthenium units linked by polycyclic aromatic hydrocarbons and heteroacenes are of special interest because of the simple synthesis methods and excellent electronic transfer properties of the bridge ligands. Kaim,[14] Low,[8,15] Zhong,[16,17] Chen,[18] and Liu[19,20] groups have performed various experiments to characterize and investigate the electronic coupling of these systems by electrochemistry, spectroelectrochemistry and theoretical calculations. Recently, we reported four isomeric benzodithiophene diethynyl diruthenium complexes and investigated their charge delocalization properties;[21] the study results revealed that benzo[1,2-b;4,5-b']-dithiophene ligand has the best charge delocalization performance (Complex **4** in Chart 1). Thus, to continually explore the relationship between bridge ligands' properties and electronic coupling based on the benzo[1,2-b;4,5-b']dithiophene ligand, we select three benzo[1,2-b;4,5-b']dithiophene analogues as bridge linkers and RuCp*dppe (Cp*＝C_5Me_5) as redox-active metal terminal, and present the synthesis, structures characterization and electronic properties of complexes **1**—**3** (Chart 1).

* E-mail: ouyaping@hynu.edu.cn
Received March 30, 2017; accepted May 21, 2017; published online June 29, 2017.
Supporting information for this article is available on the WWW under http://dx.doi.org/10.1002/cjoc.201700220 or from the author.

CHINESE JOURNAL OF CHEMISTRY

Chart 1 Benzo[1,2-b;4,5-b']dithiophene analogue-bridged bimetallic ruthenium complexes **1**—**3**

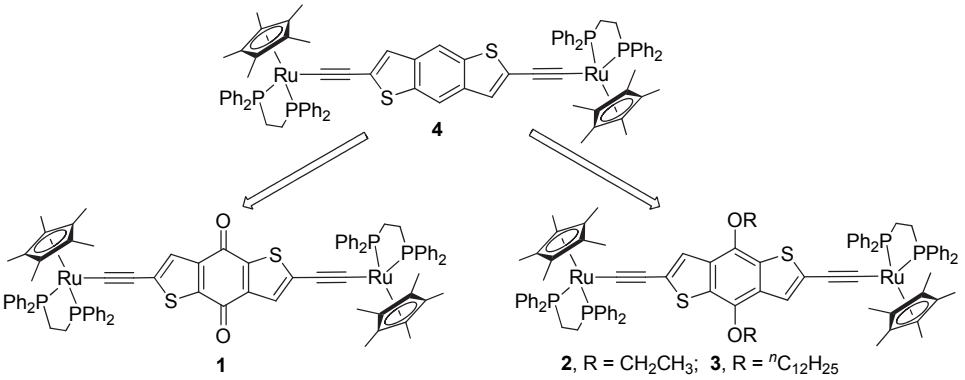

Experimental

Materials and methods

All manipulations were carried out under an atmosphere of dry argon gas by using standard Schlenk techniques, unless stated otherwise. Solvents were pre-dried, distilled and kept under an atmosphere of a dry inert gas (nitrogen or argon) prior to use in spectro-electrochemical measurements. Trimethylsilylacetylene (TMSA), $[Pd(PPh_3)_4]$, KF, $^nBu_4NBr$, CH_3CH_2Br, $^nC_{12}H_{25}Br$, Br_2, CuI and solvents were purchased from Sinopharm Chemical Reagent Co., Ltd., and used without further purification. The starting complexes [Cp*Ru(dppe)Cl],[31-33] **1a**[34] and **2a**[35] were prepared according to literature procedures.

Nuclear magnetic resonance (NMR) spectra were recorded on a Varian Mercury Plus 400 spectrometer (400 MHz) operating at 298 K in the Fourier transform mode. ^1H and ^{13}C NMR chemical shifts (δ) are relative to TMS, and ^{31}P NMR chemical shifts relative to 85% H_3PO_4. Elemental analyses (C, H, N) were performed with a Vario ElIII CHNSO instrument. Electrochemical data were obtained from cyclic voltammetry and square-wave voltammetry, using a CHI 660C potentiostat (USA) and a standard air-tight three-electrode cell. The concentrations of the analyte (complexes **1**—**3**) and supporting electrolyte (Bu_4NPF_6) were typically 10^{-3} and 10^{-1} mol•L^{-1}, respectively. A pre-polished 500-μm diameter platinum disk working electrode, a platinum wire counter electrode, and an Ag/Ag^+ reference electrode were used. Spectroelectrochemical experiments at room temperature were performed with an air-tight optically transparent thin-layer electrochemical (OTTLE) cell (optical path length of *ca.* 200 μm) equipped with a Pt minigrid working electrode and CaF_2 windows.[36] The cell was positioned in the sample compartments of a Bruker Tensor FT-IR spectrometer (1 cm^{-1} spectral resolution, 8 scans) and a Shimadzu UV-3600 UV-vis-NIR spectrophotometer. The controlled-potential electrolyses within the OTTLE cell were carried out using a CHI 660C potentiostat.

DFT calculations were performed with the Gaussian 09 program, at the B3LYP/3-21G* levels of theory. Geometry optimizations were performed without any symmetry constraints, and frequency calculations on the resulting optimized geometries showed no imaginary frequencies. Electronic transitions were calculated by the time-dependent DFT (TD-DFT) method. The MO contributions were generated using the Multiwfn2.6.1_bin_Win package and plotted using GaussView 5.0.

Preparation of intermediate compounds (1b, 2b—2d, 3b—3d)

Preparation of 2,6-bis(trimethylsilylethynyl)-1,5-dithia-s-indacene-4,8-dione (1b) To a stirred solution of 2,6-dibromo-1,5-dithia-s-indacene-4,8-dione **2a** (200 mg, 0.53 mmol), CuI (10 mg, 0.053 mmol) and $Pd(PPh_3)_4$ (61 mg, 0.053 mmol) in triethylamine (10 mL) and THF (20 mL) under an argon atmosphere was added (trimethylsilyl)acetylene (207 mg, 2.12 mmol), and the mixture was refluxed at 60 ℃ for 24 h. The cold solution was filtered through a bed of Celite. The filtrate was evaporated under reduced pressure and purified by silica gel column chromatography (CH_2Cl_2/petroleum ether, V∶V=1∶2) to give a light yellow solid (114 mg, 51%). ^1H NMR (400 MHz, $CDCl_3$) δ: 0.28 (s, 18H, $SiMe_3$), 7.63 (s, 2H).

Preparation of 4,8-diethoxybenzo[1,2-b:4,5-b']dithiophene (2b) Under an argon atmosphere, water (50 mL) was added to benzo[1,2-b:4,5-b']dithiophene-4,8-dione (1.32 g, 6.00 mmol), zinc power (819 mg, 12.6 mmol), sodium hydroxide (3.60 g, 90 mmol) in a round botom flask (100 mL). After refluxing for 3 h, to the stirred solution was added bromoethane (1.96 g, 18 mmol), $^nBu_4NBr$ (193.4 mg, 0.6 mmol). The reaction mixture was refluxed for 6 h again and then poured into water (100 mL). The mixture was extracted with diethyl ether three times. The combined organic layer was dried with anhydrous sodium sulfate and evaporated under reduced pressure and purified by silica gel column chromatography (CH_2Cl_2/petroleum ether, V∶V=1∶3) to give a white solid (1.12g, 67%). ^1H NMR (400 MHz, $CDCl_3$) δ: 1.49 (t, J=7.2 Hz, 6H, CH_3), 4.37 (q, J=7.2 Hz, 4H, OCH_2), 7.38 (d, J=5.6 Hz, 2H, thiophene-H), 7.48 (d, J=5.6 Hz, 2H, thiophene-H). ^{13}C NMR (100 MHz, $CDCl_3$) δ: 16.09 (CH_3), 69.42 (OCH_2), 120.29,

126.01, 130.33, 131.69, 144.17.

Preparation of 4,8-didodecyloxybenzo[1,2-b:4,5-b']dithiophene (3b) The procedure of **3b** was similar to that of **2b**. Benzo[1,2-b:4,5-b']dithiophene-4,8-dione (200 mg, 0.91 mmol), zinc power (124 mg, 1.91 mmol), sodium hydroxide (546 mg, 13.70 mmol), $^{n}C_{12}H_{25}Br$ (683 mg, 2.73 mmol), $^{n}Bu_4NBr$ (30 mg, 0.091 mmol), water (15 mL). Yield: 356 mg (70%) of a light yellow solid. ^{1}H NMR (400 MHz, $CDCl_3$) δ: 0.88 (t, J=6.8 Hz, 6H, CH_3), 1.15−1.40 (m, 36H, CH_2), 1.81−1.89 (m, 4H, CH_2), 4.28 (q, J=6.4 Hz, 4H, OCH_2). 7.36 (d, J=5.6 Hz, 2H, thiophene-H), 7.48 (d, J=5.6 Hz, 2H, thiophene-H); ^{13}C NMR (100 MHz, $CDCl_3$) δ: 14.15 (CH_3), 22.73, 25.98, 29.39, 29.62, 29.65, 30.43, 31.91, 74.15 (OCH_2), 114.98, 123.10, 130.87, 131.17, 142.52.

Preparation of 2,6-dibromo-4,8-diethoxybenzo-[1,2-b:4,5-b']dithiophene (2c) To a stirred solution of 4,8-diethoxybenzo[1,2-b:4,5-b']dithiophene (**2b**) (216 mg, 0.78 mmol) in CH_2Cl_2 (20 mL) under an argon atmosphere was added a CH_2Cl_2 (10 mL) solution of bromine (0.078 mL, 1.64 mmol) by a constant pressure funnel under ice-bath, the mixture was reacted for 1−2 h at room temperature. The reaction mixture was extracted with diethyl ether three times and washed with sodium hydrogen sulfite. The combined organic layer was dried with anhydrous sodium sulfate. The filtrate was evaporated under reduced pressure and purified by silica gel column chromatography (CH_2Cl_2/petroleum ether, V∶V=1∶4) to give a white solid (152 mg, 45%). ^{1}H NMR (400 MHz, $CDCl_3$) δ: 1.46 (t, J=7.2 Hz, 6H, CH_3), 4.28 (q, J=6.8 Hz, 4H, OCH_2), 7.44 (s, 2H); ^{13}C NMR (100 MHz, $CDCl_3$) δ: 16.04 (CH_3), 69.68 (OCH_2), 115.02, 123.12, 131.04, 131.37, 142.26.

Preparation of 2,6-dibromo-4,8-didodecyloxybenzo[1,2-b:4,5-b']dithiophene (3c) The procedure of **3c** was similar to that of **2c**. 4,8-Didodecyloxybenzo[1,2-b:4,5-b']dithiophene (**3b**) (2.20 g, 3.9 mmol), Br_2 (8.2 mmol, 0.4 mL), CH_2Cl_2 (100 mL). Yield 1.69 g (60%) of a white solid. ^{1}H NMR (400 MHz, $CDCl_3$) δ: 0.88 (t, J=6.8 Hz, 6H, CH_3), 1.16−1.44 (m, 36H, CH_2), 1.46−1.61 (m, 4H, CH_2), 4.17 (q, J=6.4 Hz, 4H, OCH_2). 7.42 (s, 2H, thiophene-H); ^{13}C NMR (100 MHz, $CDCl_3$) δ: 14.16 (CH_3), 22.70, 25.95, 29.37, 29.60, 29.64, 30.40, 31.92, 74.16 (OCH_2), 114.95, 123.09, 130.85, 131.13, 142.49.

Preparation of 2,6-bis(trimethylsilylethynyl)-4,8-diethoxybenzo[1,2-b:4,5-b']dithiophene (2d) To a stirred solution of 2,6-dibromo-4,8-diethoxybenzo-[1,2-b:4,5-b']dithiophene (**2c**) (370 mg, 0.85 mmol), CuI (16 mg, 0.085 mmol), and $Pd(PPh_3)_4$ (98 mg, 0.085 mmol) in triethylamine (15 mL) and THF (25 mL) under an argon atmosphere was added (trimethylsilyl)-acetylene (0.48 mL, 3.39 mmol), and the mixture was refluxed at 60 ℃ for 24 h. The cold solution was filtered through a bed of Celite. The filtrate was evaporated under reduced pressure and purified by silica gel column chromatography (CH_2Cl_2/petroleum ether, V∶V=1∶2) to give a white solid (180 mg, 45%). ^{1}H NMR (400 MHz, $CDCl_3$) δ: 0.28 (s, 18H, $SiMe_3$), 1.46 (t, J=7.2 Hz, 6H, CH_3), 4.30 (q, J=7.2 Hz, 4H, CH_2), 7.58 (s, 2H); ^{13}C NMR (100 MHz, $CDCl_3$) δ: −0.25 ($SiMe_3$), 14.20 (CH_3), 73.25 (OCH_2), 97.89 (C≡C), 102.15 (C≡C), 122.78, 124.90, 130.24, 130.96, 144.17.

Preparation of 2,6-bis(trimethylsilylethynyl)-4,8-didodecyloxybenzo[1,2-b:4,5-b']dithiophene (3d) The procedure of **3d** was similar to that of **2d**. 2,6-Dibromo-4,8-didodecyloxybenzo[1,2-b:4,5-b']dithiophene (**3c**) (200 mg, 0.28 mmol), $Pd(PPh_3)_4$ (32 mg, 0.028 mmol), CuI (5 mg, 0.028 mmol), (trimethylsilyl)acetylene (0.36 mL, 2.8 mmol), THF (20 mL), Et_3N (15 mL). Yield: 168 mg (80%) of a white solid. ^{1}H NMR (400 MHz, $CDCl_3$) δ: 0.29 (s, 18H, $SiMe_3$), 0.88 (t, J=6.8 Hz, 6H, CH_3), 1.10−1.42 (m, 32H, CH_2), 1.46−1.52 (m, 4H, CH_2), 1.82−1.87 (m, 4H, CH_2), 4.21 (q, J=6.8 Hz, 4H, OCH_2), 7.57 (s, 2H, thiophene-H); ^{13}C NMR (100 MHz, $CDCl_3$) δ: −0.25 ($SiMe_3$), 14.14 (CH_3), 22.69, 25.94, 29.42, 29.64, 30.45, 31.92, 74.14 (OCH_2), 97.96 (C≡C), 101.63 (C≡C), 122.82, 125.96, 130.17, 131.74, 143.81.

Preparation of bimetal ruthenium acetylide complexes 1−3

Preparation of 1 A solution of Cp*(dppe)RuCl (341 mg, 0.51 mmol), 2,6-bis(trimethylsilylethynyl)-1,5-dithia-s-indacene-4,8-dione (**1b**) (100 mg, 0.24 mmol), and KF (168 mg, 2.90 mmol) in 20 mL CH_3OH and 5 mL THF was heated to reflux under nitrogen atmosphere for 24 h. The crude product was collected by filtration, washed with methanol and hexane. The solid was dissolved in dichloromethane and precipitated from slow diffusion with hexane. The solid was filtered and dried to give **1** as an atrovirens solid (216 mg, 55%). ^{1}H NMR (400 MHz, $CDCl_3$) δ: 1.54 (s, 30H, $2C_5(CH_3)_5$), 2.07 (br, 4H, $CH_{2/dppe}$), 2.63 (br, 4H, $CH_{2/dppe}$), 6.65 (s, 2H), 7.20−7.37 (m, 32H, $H_{Ar/dppe}$), 7.66 (br, 8H, $H_{Ar/dppe}$); ^{13}C NMR (100 MHz, $CDCl_3$) δ: 9.90 (CH_3), 29.34 (t, J=22.90 Hz, $CH_{2/dppe}$), 93.61 (C/C_5Me_5), 106.71 (s, thiophene-C≡C), 123.59(Ru-C≡CH), 127.57, 129.21, 129.34, 133.19, 135.82, 136.31, 137.84, 138.18, 140.80, 145.03, 159.00, 174.28 (C=O); ^{31}P NMR (160 MHz, $CDCl_3$) δ: 79.09 (dppe). Anal. calcd for $C_{92}H_{98}O_2P_4Ru_2S_2$: C 67.96, H 6.08; found C 67.91, H 6.12.

Preparation of 2 The procedure of **2** was similar to that of **1**. Cp*(dppe)RuCl (388 mg, 0.58 mmol), 2,6-bis(trimethylsilylethynyl)-4,8-diethoxybenzo[1,2-b:4,5-b']dithiophene (**2d**) (130 mg, 0.28 mmol), KF (192 mg, 3.31 mmol), CH_3OH (20 mL), THF (5 mL). Yield: 279 mg (60%) of a brown solid. ^{1}H NMR (400 MHz, $CDCl_3$) δ: 1.46 (t, J=7.2 Hz, 6H, CH_2CH_3), 1.56 (s, 30H, $2C_5(CH_3)_5$), 2.06 (br, 4H, $CH_{2/dppe}$), 2.69 (br, 4H, $CH_{2/dppe}$), 4.17 (q, J=6.4 Hz, 4H, OCH_2), 6.50 (s, 2H), 7.23−7.38 (m, 32H, $H_{Ar/dppe}$), 7.77 (br, 8H, $H_{Ar/dppe}$); ^{13}C NMR (100 MHz, $CDCl_3$) δ: 10.04 (Cp^*-CH_3), 29.50 (m, $CH_{2/dppe}$), 68.46 (OCH_2), 92.90 (C/C_5Me_5), 103.29 (s, thiophene-C≡C), 116.32 (Ru-C≡CH), 127.41,

128.40, 128.94, 131.50, 133.21, 133.57, 136.30, 136.79, 138.64, 141.30, 142.60; ^{31}P NMR (160 MHz, $CDCl_3$) δ: 79.00 (dppe). Anal. calcd for $C_{96}H_{108}O_2P_4Ru_2S_2$: C 68.47, H 6.46; found C 68.57, H 6.30.

Preparation of 3 The procedure of **3** was similar to that of **1**. Cp*(dppe)RuCl (244 mg, 0.36 mmol), 2,6-bis(trimethylsilylethynyl)-4,8-didodecyloxybenzo[1,2-b:4,5-b']dithiophene (**3d**) (130 mg, 0.17 mmol), KF (121 mg, 2.07 mmol), CH_3OH (20 mL), THF (5 mL). Yield: 231 mg (68%) of a brownish black solid. ^{1}H NMR (400 MHz, $CDCl_3$) δ: 0.86 (t, J=6.8 Hz, 6H, CH_3), 1.20—1.35 (m, 32H, CH_2), 1.37—1.47 (m, 4H, CH_2), 1.78—1.92 (m, 4H, CH_2), 2.07 (br, 4H, $CH_{2/dppe}$), 2.65 (br, 4H, $CH_{2/dppe}$), 4.08 (q, J=6.8 Hz, 4H, OCH_2), 6.52 (s, 2H, thiophene-H), 7.24—7.40 (m, 32H, $H_{Ar/dppe}$), 7.78 (br, 8H, $H_{Ar/dppe}$); ^{13}C NMR (100 MHz, $CDCl_3$) δ: 10.00 (Cp^*-CH_3), 14.14 (CH_3), 22.68, 26.23, 29.38, 29.76, 30.62, 30.94, 31.91, 73.08 (OCH_2), 92.86 (C/C_5Me_5), 103.20 (thiophene-C≡C), 116.29 (Ru-C≡C), 127.40, 128.20, 128.96, 129.36, 131.31, 133.20, 133.57, 136.27, 136.76, 138.24, 138.58, 141.53, 142.28; ^{31}P NMR (160 MHz, $CDCl_3$) δ: 79.04 (dppe). Anal. calcd for $C_{116}H_{148}O_2P_4Ru_2S_2$: C 70.92, H 7.59; found C 70.88, H 7.70.

Results and Discussion

Syntheses and characterization

The general synthetic routes for the preparation of intermediate compounds **1b**, **2d** and **3d** and bimetal ruthenium acetylide complexes **1**—**3** are outlined in Schemes 1, 2. Precursor molecules **1b**, **2d** and **3d** were prepared by the previously reported methods.[22-24] Subsequently, the TMS termini of compounds **1b**, **2d** and **3d** were deprotected in methanolic KF solution and not separated further, and reacted with [RuCl(dppe)Cp*] in one pot at 60 ℃.[8] Complexes **1**—**3** were synthesized in moderate yields, and the structures were characterized by NMR (^{1}H, ^{13}C and ^{31}P). Notable close proton resonance signals from dppe (δ 2.07 and 2.69) and C_5Me_5 (δ 1.55) and very similar shifts of ^{31}P resonance signal (δ 79) of dppe were found in respective ^{1}H and ^{31}P NMR spectra of complexes **1**—**3**. ^{13}C NMR spectra show that the shifts (δ 103.29 and 116.32) of the acetylenic carbon atoms of **1** differ from those of complexes **2** and **3**.

Scheme 1 Synthetic route for the preparation of intermediate compounds **1b**, **2d** and **3d**

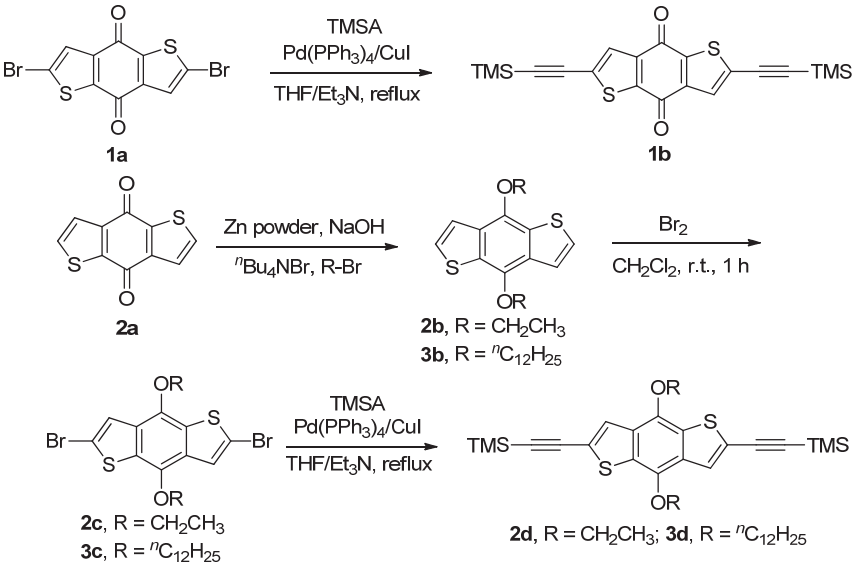

Scheme 2 Synthetic route for the preparation of target complexes **1**—**3**

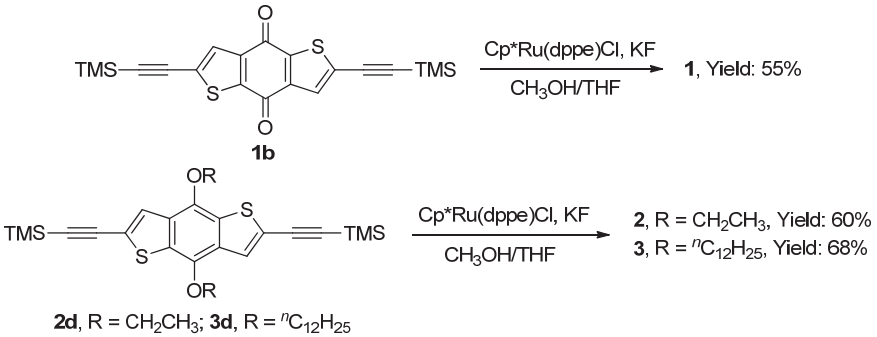

Electrochemical studies

In order to understand the redox properties of complexes **1**—**3** with the identical metal redox-active terminal group "Cp*(dppe)RuC≡C—" and bridge ligands of different electronic properties, electrochemistry was explored by anodic cyclic voltammogram (CV) and square-wave voltammograms (SWV) in dry CH_2Cl_2/0.1 mol•L^{-1} Bu_4NPF_6 to investigate their redox processes and electronic coupling properties (Figure 1 and Table 1). Complexes **1**—**3** display two reversible redox events between −0.4 and 0.4 V (Figures 1a and 1b) with redox separations ($\Delta E_{1/2}=E_{1/2}^{(2)}-E_{1/2}^{(1)}$) of 96 mV (**1**), 140 mV (**2**) and 143 mV (**3**), respectively, which indicates different charge delocalization degree over the molecule framework under the same external conditions (*i.e.*, solvent, supporting electrolyte, sample concentration, temperature and so on). Furthermore, additional electrode processes at higher *E* are only seen for complexes **2** and **3** rather than for **1** in Figure 1 (0.6—1.0 V), which may be likely attributable to electrochemical behavior from thiophene rings of bridge ligands.[25]

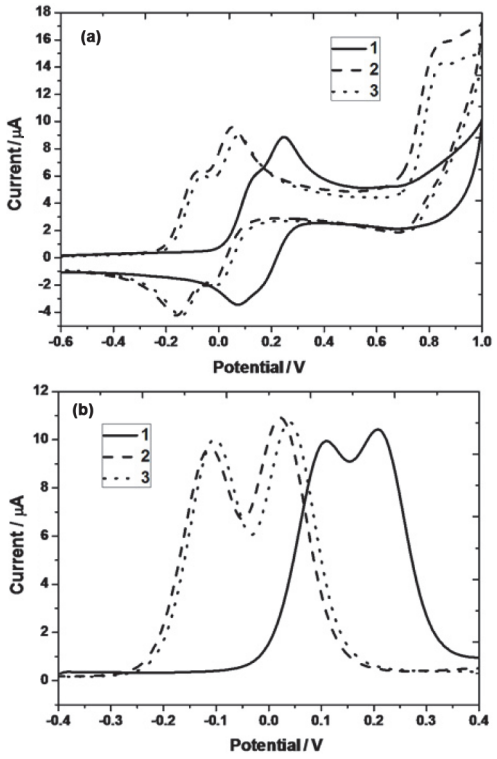

Figure 1 (a) Cyclic voltammograms (CV) of complexes **1**—**3** in CH_2Cl_2/Bu_4NPF_6 at $v=10^{-1}$ V•s^{-1} and (b) anodic square-wave voltammograms (SWV) of complexes **1**—**3** at $f=10$ Hz.

Viewing from the electrochemical data, complex **1** with an electron deficient and less well-conjugated bridge (cross-conjugation) exhibits an evidently larger half-wave potential than that of the reported complex **4**,[21] and smaller $\Delta E_{1/2}$ value. However, complexes **2** and **3** with alkoxyl groups are derived from reported complex **4**, in which the half-wave potentials and $\Delta E_{1/2}$ value slightly increase compared with complex **4**. The electrochemical behavior of complexes **2** and **3** is identical with very minor potential shifts resulting from the different alkoxy substituents. These results reveal that electronic effect and conjugative degree influence the redox potential value and the charge transfer abilities of bridge ligands. Generally speaking, bridge ligands of more electron-rich and better conjugated bridge ligands improve the charge delocalization, whereas the length of substituent chains in bridge ligands only displays minimal effect.

Table 1 Electrochemical data for complexes **1**—**3**[a]

Complex	$E_{1/2}^{(1)}$/V	$E_{1/2}^{(2)}$/V	$\Delta E_{1/2}$[b]/mV
1	0.110	0.206	96
2	–0.115	0.025	140
3	–0.102	0.041	143
4[21]	–0.124	0.016	140

[a] Anodic potentials in Volt vs. Fc/Fc^+ obtained from cyclic voltammograms recorded at 298 K in dichloromethane/10^{-1} mol•L^{-1} Bu_4NPF_6. Additional electrochemical processes observed at higher electrode potentials were not listed further. [b] $\Delta E_{1/2}=E_{1/2}^{(2)}-E_{1/2}^{(1)}$ denotes the potential difference between the two reversible anodic processes.

IR spectroelectrochemical studies

IR spectra have been used to explore structural changes on the bridge ligands, which contain the characteristic groups (C≡C) in complexes **1**—**3**. Guided by the cyclic voltammetry results, we carried out IR spectroelectrochemical investigation on diruthenium ethynyl complexes $\mathbf{1}^{n+}$—$\mathbf{3}^{n+}$($n=0$, 1, 2) electrochemically generated in $CH_2Cl_2/10^{-1}$ mol•L^{-1} Bu_4NPF_6 within OTTLE cell. Figure 2 illustrates the spectral curve in the IR ν(C≡C) regions for complexes $\mathbf{1}^{n+}$($n=0$ (solid), 1 (broken), 2 (dotted)), and IR spectral change processes in the ν(C≡C) region recorded during the oxidation $\mathbf{2}\rightarrow\mathbf{2}^{+}\rightarrow\mathbf{2}^{2+}$ and $\mathbf{3}\rightarrow\mathbf{3}^{+}\rightarrow\mathbf{3}^{2+}$ are exhibited in Figure 3 and Figure S1 (Supporting Information), respectively.

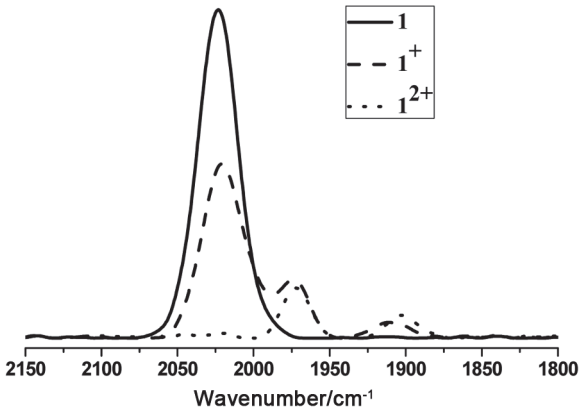

Figure 2 Spectral changes in the IR ν(C≡C) regions recorded for complexes $\mathbf{1}^{n+}$ ($n=0$ (solid), 1 (broken), 2 (dotted)) electrochemically generated in $CH_2Cl_2/10^{-1}$ mol•L^{-1} Bu_4NPF_6 at 298 K within an OTTLE cell.

CHINESE JOURNAL OF CHEMISTRY

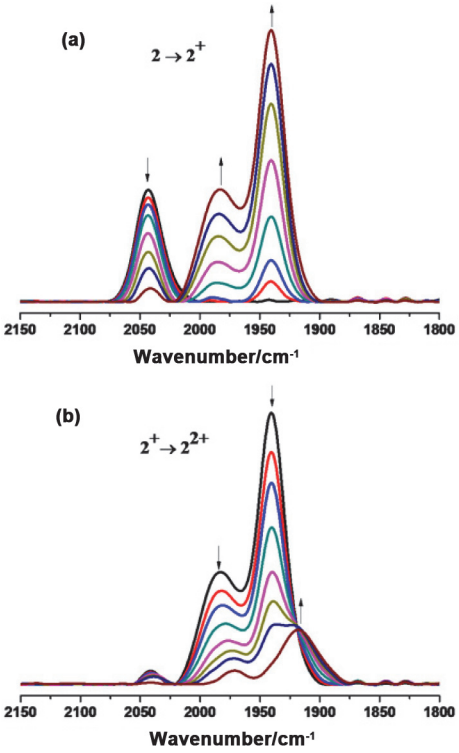

Figure 3 IR spectra changes in ν(C≡C) region recorded during the oxidation **2**→**2**$^{+}$ (a) and **2**$^{+}$→**2**$^{2+}$ (b) in $CH_2Cl_2/10^{-1}$ mol•L^{-1} *n*-Bu_4NPF_6 at 298 K within an OTTLE cell.

Complex **1** with electron-deficient bridge ligands and poor conjugation (cross-conjugation), exhibits the IR *ν*(C≡C) absorption at lower energy band (2023 cm^{-1}) than **2**, **3** (2043 cm^{-1}). The absorption at 2023 cm^{-1} decreased along with appearance of two other weak bands at 1974 and 1909 cm^{-1} (Table 2), indicating that the charge is located in a C≡C band from the bridge ligand. IR spectral changes in the redox process from complexes **2** and **3** that adhered to alkoxy chains are similar to that of complex **4**. Only the *ν*(C≡C) absorptions of singly oxidized states **2**$^{+}$ and **3**$^{+}$ exhibit a low-energy shift (**2**$^{+}$ and **3**$^{+}$: 1984 cm^{-1}, 1941 cm^{-1}), showing larger ν(C≡C) absorption shift ($\Delta\nu$=102 cm^{-1}). These results reveal that electron-rich bridge ligands are favorable for charge delocalization. With the continuous oxidation of monocations with respect to dications, complex **1**$^{2+}$ exhibits two weak absorptions at 1972 and 1902 cm^{-1}, while complexes **2**$^{2+}$ and **3**$^{2+}$ both show a weak absorption at around 1917 cm^{-1}. These changes from complexes **2**—**4** feature the IR spectral characteristics of analogous diruthenium ethynyl complexes bridged by conjugating highly electron-rich ligands.[8,19,21]

Table 2 Spectroelectrochemically determined *ν*(C≡C) wavenumbers (cm^{-1}) for **1**$^{n+}$—**3**$^{n+}$(*n*=0, 1, 2)

Complex	Freq.	*n*=0	*n*=1	*n*=2
1^{n+}	*ν*(C≡C)	2023 (s)	2022 (s), 1974 (w), 1909 (w)	1972 (w), 1902 (w)
2^{n+}	*ν*(C≡C)	2043 (s)	1984 (s), 1941 (vs)	1917 (w)
3^{n+}	*ν*(C≡C)	2043 (s)	1984 (s), 1941 (vs)	1918 (w)

UV-vis-NIR spectroelectrochemical studies

Further UV-vis-NIR spectroelectrochemical experiments are carried out by using an OTTLE cell in $CH_2Cl_2/10^{-1}$ mol•L^{-1} *n*-Bu_4NPF_6 at 298 K to gain deeper insight into the redox processes of complexes **1**—**3**. UV-vis-NIR spectra of complexes [**1**]$^{n+}$ (*n*=0, 1, 2) were recorded between 250 and 2000 nm, which is displayed in Figure 4 and corresponding spectral traces recorded throughout the electrolysis process from **1**→**1**$^{+}$→**1**$^{2+}$ are shown in Figure S3 (Supporting Information), and the UV-vis-NIR spectral changes for reversibly oxidized complexes **2** and **3** are shown in Figures 5 and S2 (Supporting Information), respectively. The characteristic electron absorption spectra data are presented in Table 3.

Table 3 UV-vis-NIR absorption data for **1**$^{n+}$—**3**$^{n+}$(*n*=0, 1, 2)

Complex	UV/vis/NIR absorption λ_{max}/nm (10^{-4} ε_{max}/(dm^3•mol^{-1}•cm^{-1}))
1	403 (4.23), 665 (1.61)
1^{+}	389 (2.18), 733 (0.82)
1^{2+}	328 (2.89), 733 (0.46)
2	435 (6.54)
2^{+}	435 (1.72), 650 (2.13), 2131 (1.81)
2^{2+}	920 (2.74)
3	435 (6.59)
3^{+}	441 (1.64), 655 (1.88), 2134 (1.56)
3^{2+}	570 (0.90), 919 (2.99)

Neutral complexes **1**—**3** displayed intense absorptions between 400 nm and 450 nm in the UV-vis region which are based on ligand-centered π → π* transitions, while complex **1** also exhibited another absorption at 665 nm, which may be assigned to MLCT transition. Upon gradual oxidation to **1**$^{+}$—**3**$^{+}$, the intense UV absorptions of the neutral molecules decreased gradually in amplitude. The singly oxidized state **1**$^{+}$ is characterized by spectral changes with a bathochromic shift moderately at around 665 nm, and does not show any absorptions in the NIR range (Figure 4). This phenomenon further proved that the bridge ligand of complex **1** has poor charge delocalization ability. In addition, a solution of **1**$^{+}$ necessarily contains some **1** and **1**$^{2+}$ formed in a disproportionation equilibrium because of a half-wave potential separation of only 96 mV in **1** (Table 1). Therefore, the lack of an NIR band for **1**$^{+}$ may be caused by instability and poor charge delocalization of singly oxidized state **1**$^{+}$. For **2**$^{+}$ and **3**$^{+}$, a moderately intense broad band appeared in the visible region around 650 nm along with the occurrence of a broad near-infrared absorption between 1200 nm and 3000 nm (Figure 5). The two bands are attributed respectively to LMCT and MLCT transitions on the basis of TDDFT

calculations (see below). The broad absorption bands of monocations $\mathbf{2}^{+}$ and $\mathbf{3}^{+}$ may be deconvoluted into the sum of several Gaussian-shaped sub-bands by reports about similar diruthenium ethynyl complexes,[8,26,27] which are caused by different orbital transitions. However, Kaupp and Low *et al*.[28-30] have performed various experiments and theoretical calculations, and concluded that the broad NIR absorptions are due to overlapping transitions of several rotamers coexisiting in equilibrium.

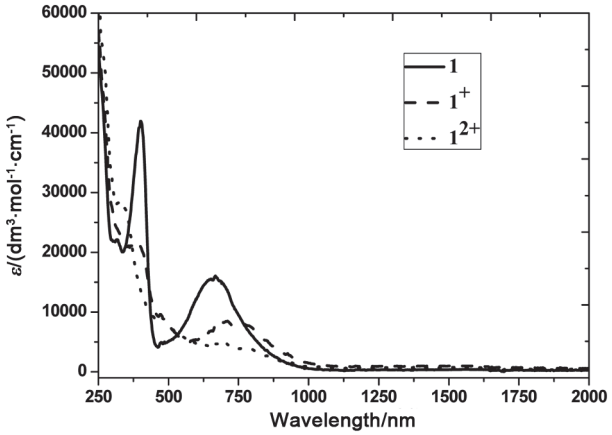

Figure 4 The UV-vis-NIR spectra of $[\mathbf{1}]^{n+}$ (n=0, 1, 2) collected by *in situ* oxidation of **1** in dichloromethane at 293 K within an OTTLE cell.

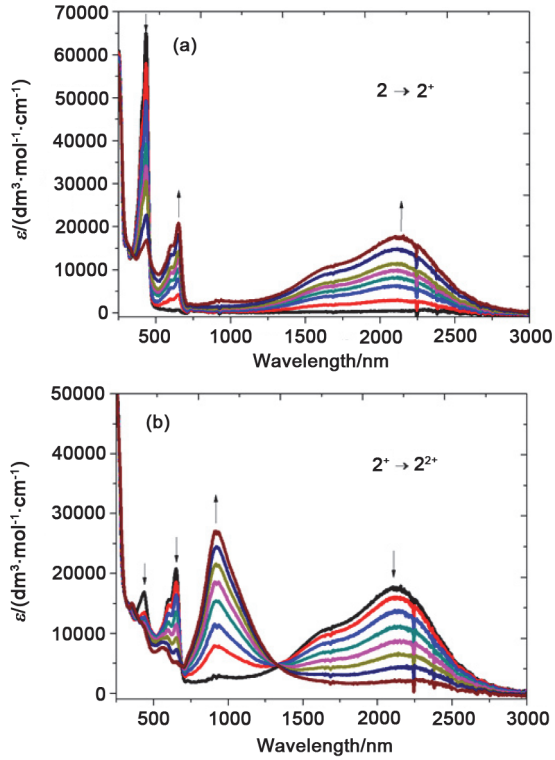

Figure 5 UV-vis-NIR spectral changes recorded during the oxidation $\mathbf{2}\rightarrow\mathbf{2}^{+}$ (a) and $\mathbf{2}^{+}\rightarrow\mathbf{2}^{2+}$ (b) in $CH_2Cl_2/10^{-1}$ mol/L n-Bu_4NPF_6 at 298 K within an OTTLE cell.

With further oxidation to dicationic $\mathbf{1}^{2+}$—$\mathbf{3}^{2+}$, a new strong absorption band appeared in a visible region between 700 nm and 1000 nm for $\mathbf{2}^{2+}$ and $\mathbf{3}^{2+}$, respectively. The analysis shows that the spectroscopic changes of complexes **2** and **3** during the redox processes are similar to that of benzo[1,2-b;4,5-b']dithiophene ethynyl-bridged diruthenium complex **4**.[21] During the formation of complex $\mathbf{1}^{2+}$, the relative absorptions at 389 and 733 nm decrease to a minimum level.

DFT and TDDFT calculations

In order to shed light on the electronic characters of monocations $\mathbf{1}^{+}$ and $\mathbf{2}^{+}$, density functional theory (DFT) calculations were performed on model complexes $[\mathbf{1\text{-}H}]^{+}$ and $[\mathbf{2\text{-}H}]^{+}$ according to previous studies on similar systems[8, 26] on the level of theory of B3LYP/3-21G*, where "-H" indicated that η^5-C_5Me_5 (Cp*) and dppe were replaced by η^5-C_5H_5 (Cp) and two PH_3 ligands. The selected frontier orbitals of $\mathbf{[1\text{-}H]}^{+}$ and $\mathbf{[2\text{-}H]}^{+}$ are shown in Figure 6. Lists of corresponding frontier molecular orbital energies and compositions from Mulliken analysis are provided in Tables S1—S2 (Supporting Information), respectively. The β-LUSO and α-LUSO orbitals of $\mathbf{[1\text{-}H]}^{+}$ and $\mathbf{[2\text{-}H]}^{+}$ displayed certain similarity and are delocalized over the whole molecule skeleton with larger proportions from conjugated bridge moieties ($\mathbf{[1\text{-}H]}^{+}$: 66%; $\mathbf{[2\text{-}H]}^{+}$: 78%) and smaller contributions from ruthenium end groups ($\mathbf{[1\text{-}H]}^{+}$: 34%; $\mathbf{[2\text{-}H]}^{+}$: 22%). In comparison, $\mathbf{[2\text{-}H]}^{+}$ bridged by benzo[1,2-b;4,5-b']dithiophene derivative displays larger bridge ligand character, which revealed the excellent charge delocalization of substituted benzo[1,2-b;4,5-b′]dithiophene. This can also be clearly proved by the spin density distribution in Figure 7, where the contributions of the bis(ethynyl) substituted bridging ligand dominate largely over those of the metal termini.

Time-dependent DFT (TDDFT) calculations were performed at the level of B3LYP/3-21G* on the singly-oxidized species $[\mathbf{1\text{-}H}]^{+}$ and $[\mathbf{2\text{-}H}]^{+}$ to aid in the assignment of the spectra of complexes $\mathbf{1}^{+}$and $\mathbf{2}^{+}$. The details for major electronic excitations of singly-oxidized $\mathbf{[1\text{-}H]}^{+}$ and $\mathbf{[2\text{-}H]}^{+}$ are delineated in Table 4, and the corresponding isosurface plots of molecular orbitals involved in the major electronic excitations are depicted in Figure S4 (Supporting Information). For complex $\mathbf{[1\text{-}H]}^{+}$, the results from TDDFT calculations show that the two absorptions in the UV-vis region most likely have large contributions from α-HOSO-1→α-LUSO and β-HOSO-10→β-LUSO, which are assigned to LMCT and M-C≡C→LCT transitions, respectively. However, the transition at 2387 nm predicted by TDDFT calculations was not matched by a close NIR absorption, which may be attributable to the instability of $\mathbf{[1]}^{+}$. TD-DFT calculations with monocation $\mathbf{[2\text{-}H]}^{+}$ reveal two high-energy transitions (507 nm: α-HOSO→α-LUSO; 525 nm: β-HOSO-7→β-LUSO) which have bridge π→π* and LMCT character respectively. In addition, a low-energy (near-IR) excita-

CHINESE JOURNAL OF CHEMISTRY

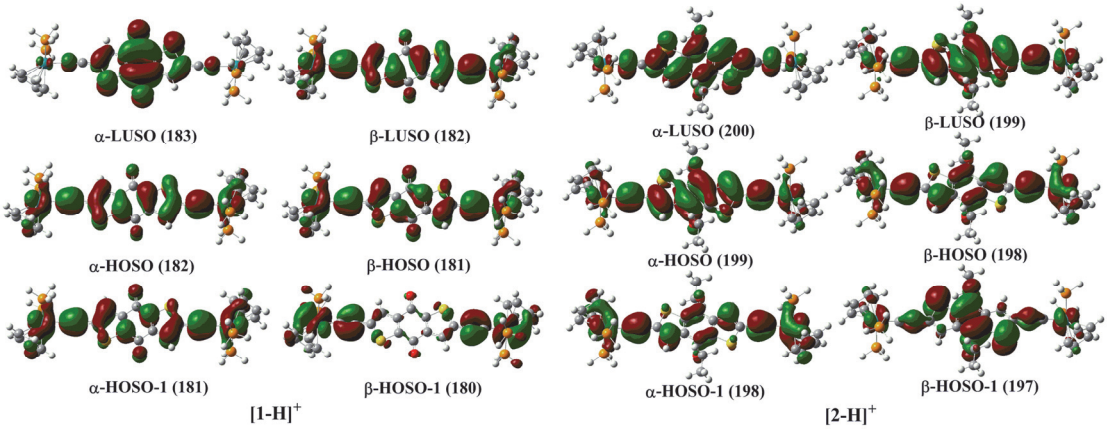

Figure 6 Selected molecular orbitals of model complexes **[1-H]**$^+$and **[2-H]**$^+$ plotted with contour values $\pm$0.04 (e/bohr^3)$^{1/2}$.

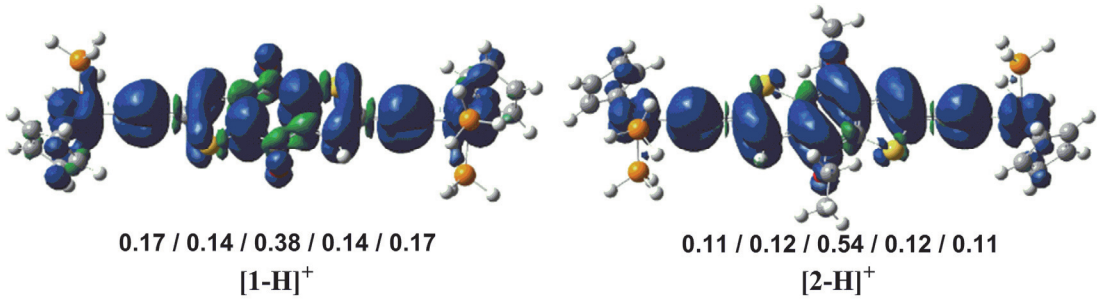

Figure 7 Spin-density distributions in [**1-H**]$^+$and [**2-H**]$^+$ (Ru/CH≡CH/Bridge cores/CH≡CH/Ru) with the corresponding compositions. Contour values: $\pm$0.04 (e/bohr^3)$^{1/2}$.

Table 4 Major electronic excitations of singly-oxidized **[1-H]**$^+$ and **[2-H]**$^+$ determined by TD-DFT methods

Complex	Energy/cm^{-1}	λ/nm	f	Major contribs	Assignment
	4189	2387	0.3203	β-HOSO→β-LUSO (100%)	Bridge π→π* mixed with MLCT
[1-H]$^+$	17316	578	0.3628	β-HOSO-10→β-LUSO (67%)	LMCT
	18345	545	0.2713	α-HOSO-1→α-LUSO (55%)	M-C≡C→LCT
	8737	1145	0.6760	β-HOSO→β-LUSO (98%)	M-C≡C→LCT
[2-H]$^+$	19062	525	0.3628	β-HOSO-7→β-LUSO (82%)	LMCT
	19720	507	0.7935	α-HOSO→α-LUSO (75%)	Bridge π→π*

tion arising from the β-HOSO→β-LUSO transition at 1145nm was found, which can be likely responsible for the lower energy broad absorption band observed in the experimental spectra and feature larger M-C≡C→LCT character. However, numerous studies have been conducted by Kaupp, Low and Liu *et al.*, which have proven that similar broad NIR absorptions are composed of several sub-bands caused by different rotameric forms.[19,21,28-30]

Conclusions

Dinuclear ruthenium complexes **1**—**3** bridged by 1,5-dithia-s-indacene-4,8-dione, 4,8-diethoxybenzo[1,2-b:4,5-b']dithiophene and 4,8-didodecyloxybenzo[1,2-b:4,5-b']dithiophene ligands were prepared and characterized using NMR and elemental analysis. Redox and electronic properties of complexes **1**—**3** were investigated by cyclic voltammetry, square-wave voltammograms and spectroelectrochemical methods. Redox potential separations (ΔE) of 96 mV (**1**), 140 mV (**2**) and 143 mV (**3**) have been observed, and suggest weaker charge delocalization in complex **1** than those of complexes **2** and **3**. Stepwise spectroelectrochemical oxidation of **1**—**3** produced spectroscopic signatures of singly oxidized species **[1]**$^+$—**[3]**$^+$. Furthermore, IR spectroelectrochemical results revealed larger ν(C≡C) absorption separation ($\Delta\nu$=102 cm^{-1}) from neutral states to monocations for complexes **2** and **3**, and no ν(C≡C) shifts at **1**→**1**$^+$. In addition, only for **2**$^+$ and **3**$^+$, a broad near-infrared absorption between 1200 nm and 3000 nm was recorded, which was assigned by TDDFT calculations. Above results concluded that [1,2-b:4,5-b']dithiophene derivatives bridged diruthenium complexes **2** and **3** exhibit more excellent charge delocalization abili-

ties than complex **1**, and further strengthened the evidence linking bridge ligands properties with redox and electronic coupling.

Acknowledgement

The authors acknowledge financial support from National Natural Science Foundation of China (No. 21602049) and the Natural Science Foundation of Hunan Province, China (No. 2017JJ3004).

References

[1] Ward, M. D. *Chem. Soc. Rev*. **1995**, *24*, 121.
[2] Launay, J. P. *Chem. Soc. Rev*. **2001**, *30*, 386.
[3] Ceccon, A.; Santi, S.; Orian, L.; Bisello, A. *Coord. Chem. Rev*. **2004**, *248*, 683.
[4] Aguirre-Etcheverry, P.; O'Hare, D. *Chem. Rev*. **2010**, *110*, 4839.
[5] Liu, S. H.; Hu, Q. Y.; Xue, P.; Wen, T. B.; Williams, I. D.; Jia, G. *Organometallics* **2005**, *24*, 769.
[6] Qi, H.; Gupta, A.; Noll, B. C.; Snider, G. L.; Lu, Y.; Lent, C.; Fehlner, T. P. *J. Am. Chem. Soc*. **2005**, *127*, 15218.
[7] Wu, X. H.; Jin, S.; Liang, J. H.; Li, Z. Y.; Yu, G.-A.; Liu, S. H. *Organometallics* **2006**, *28*, 2450.
[8] Fox, M. A.; Guennic, B. L.; Roberts, R. L.; Brue, D. A.; Yufit, D. S.; Howar, J. A. K.; Manca, G.; Halet, J. F.; Hartl, F.; Low, P. J. *J. Am. Chem. Soc*. **2011**, *133*, 18433.
[9] Shah, H. H.; Al-Balushi, R. A.; Al-Suti, M. K.; Khan, M. S.; Woodall, C. H.; Molloy, K. C.; Raithby, P. R.; Robinson, T. P.; Dale, S. E. C.; Marken, F. *Inorg. Chem*. **2013**, *52*, 4898.
[10] Justaud, F.; Gendron, F.; Ogyu, Y.; Kumamoto, Y.; Miyazaki, A.; Ouahab, L.; Costuas, K.; Halet, J.-F.; Lapinte, C. *Chem. Eur. J*. **2013**, *19*, 5742.
[11] Scheerer, S.; Rotthowe, N.; Abdel-Rahman, O. S.; He, X.; Rigaut, S.; Kvapilová, H.; Záliš, S.; Winter, R. F. *Inorg. Chem*. **2015**, *54*, 3387.
[12] Laws, D. R.; Bullock, R. M.; Lee, R.; Huang, K.-W.; Geiger, W. E. *Organometallics* **2014**, *33*, 4716.
[13] Brown, N. J.; Lancashire, H. N.; Fox, M. A.; Collison, D.; Edge, R.; Yufit, D. S.; Howard, J. A. K.; Whiteley, M. W.; Low, P. J. *Organometallics* **2011**, *30*, 884.
[14] Kaim, W.; Lahiri, G. K. *Angew. Chem., Int. Ed*. **2007**, *46*, 1778.
[15] Low, P. J. *Coord. Chem. Rev*. **2013**, *257*, 1507.
[16] Yao, C.-J.; Zhong, Y.-W.; Yao, J. *J. Am. Chem. Soc*. **2011**, *133*, 15697.
[17] Wang, L.; Yang, W.-W.; Zhong, Y.-W.; Yao, J. *Dalton Trans*. **2013**, *42*, 5611.
[18] Gao, L.-B.; Kan, J.; Fan, Y.; Zhang, L.-Y.; Liu, S.-H.; Chen, Z.-N. *Inorg. Chem*. **2007**, *46*, 5651.
[19] Zhang, J.; Zhang, M.-X.; Sun, C.-F.; Xu, M.; Hartl, F.; Yin, J.; Yu, G.-A.; Rao, L.; Liu, S. H. *Organometallics* **2015**, *34*, 3967.
[20] Ou, Y.-P.; Jiang, C.; Wu, D.; Xia, J.; Yin, J.; Jin, S.; Yu, G.-A.; Liu, S. H. *Organometallics* **2011**, *30*, 5763.
[21] Ou, Y.-P.; Zhang, J.; Zhang, F.; Kuang, D.; Hartl, F.; Rao, L.; Liu, S. H. *Dalton Trans*. **2016**, *45*, 6503.
[22] Wu, X. H.; Jin, S.; Liang, J. H.; Li, Z. Y.; Yu, G.-A.; Liu, S. H. *Organometallics* **2009**, *28*, 2450.
[23] Zhang, G. B.; Fu, Y. Y.; Zhang, Q.; Xie, Z. Y. *Chem. Commun*. **2010**, *46*, 4997.
[24] Zhou, N.; Guo, X.; Ortiz, R. P.; Li, S.; Zhang, S.; Chang, R. P. H.; Facchetti, A.; Marks, T. J. *Adv. Mater*. **2012**, *24*, 2242.
[25] Ferrón, C. C.; Delgado, M. C. R.; Hernández, V.; Navarrete, J. T. L.; Vercelli, B.; Zotti, G.; Cortada, M. C.; Novoa, J. J.; Niu, W.; Hed, M.; Hartl, F. *Chem. Commun*. **2011**, *47*, 12622.
[26] Ou, Y.-P.; Xia, J.; Zhang, J.; Xu, M.; Yin, J.; Yu, G.-A.; Liu, S. H. *Chem. Asian J*. **2013**, *8*, 2023.
[27] Maurer, J.; Winter, R. F.; Sarkar, B.; Fiedlerb, J.; Záliš, S. *Chem. Commun*. **2004**, *17*, 1900.
[28] Parthey, M.; Kaupp, M. *Chem. Soc. Rev*. **2014**, *43*, 5067.
[29] Parthey, M.; Gluyas, J. B. G.; Fox, M. A.; Low, P. J.; Kaupp, M. *Chem. Eur. J*. **2014**, *20*, 6895.
[30] Renz, M.; Kess, M.; Diedenhofen, M.; Klamt, A.; Kaupp, M. *J. Chem. Theory Comput*. **2012**, *8*, 4189.
[31] Bruce, M. I.; Ellis, B. G.; Low, P. J.; Skelton, B. W.; White, A. H. *Organometallics* **2003**, *22*, 3184.
[32] Ou, Y.-P.; Zhang, J.; Kuang, D.-Z.; Zhang, F.; Yu, J.; Zhu, X. *Chin. J. Inorg. Chem*. **2016**, *32*, 641.
[33] Zhang, J.; Ou, Y.-P.; Xu, M.; Yin, J.; Yu, G.-A.; Liu, S. H. *Chin. Sci. Bull*. **2014**, *59*, 1647.
[34] Kuo, C.-Y.; Nie, W.; Tsai, H.; Yen, H.-J.; Mohite, A. D.; Gupta, G.; Dattelbaum, A. M.; William, D. J.; Cha, K. C.; Yang, Y.; Wang, L.; Wang, H.-L. *Macromolecules* **2014**, *47*, 1008.
[35] Urbani, M.; Medel, M.; Kumai, S. A.; Ince, M.; Bhaskarwar, A. N.; González-Rodríguez, D.; Grätzel, M.; Nazeeruddin, M. K.; Torres, T. *Chem.-Eur. J*. **2015**, *21*, 16252.
[36] Krejčík, M.; Daněk, M.; Hart1, F. *J. Electroanal. Chem*. **1991**, *317*, 179.

(Cheng, F.)

